Potential for non-destructive astrochemistry using the ExoMars PanCam

Michael C. Storrie-Lombardi,[1] J.-P. Muller,[2,3] M. R. Fisk,[4] A. D. Griffiths,[2,3] and A. J. Coates[2,3]

[1] We investigate the utility of adding a 365 nm ultraviolet (UV) light source to the ExoMars panoramic camera (PanCam) scheduled for launch in 2013. The modification makes it feasible to monitor rover drill cuttings for aromatic organic molecules and provide constraints on polycyclic aromatic hydrocarbons (PAH) as a function of depth to the 2-meter limit of the ExoMars drill. This non-destructive triage allows prioritized deployment of organic detection experiments requiring sample destruction and/or expenditure of non-replaceable resources. Utilizing the Beagle 2 PanCam backup filter wheel fitted with original blue (440 nm), green (530 nm), and red (670 nm) filters we captured fluorescent images following 365 nm excitation of 3-, 4- and 5-ring PAH species doped on Mars analog peridotite grains. We demonstrate a detection limit for pyrene of 1.5 μg in granular peridotite doped at pyrene levels of 50 $\pm$ 5 ppm for camera-to-target distance of 1 meter. **Citation:** Storrie-Lombardi, M. C., J.-P. Muller, M. R. Fisk, A. D. Griffiths, and A. J. Coates (2008), Potential for non-destructive astrochemistry using the ExoMars PanCam, *Geophys. Res. Lett.*, *35*, L12201, doi:10.1029/2008GL034296.

1. Introduction

[2] Broad infrared spectral emission features at 3.3, 6.2, 7.7, 8.6, 11.3, and 12.7 μm most closely matching PAH spectral signatures [*van Dishoeck*, 2004] are found in the interstellar medium (ISM) of nearby star forming regions [*Ehrenfreund and Charnley*, 2000], around protoplanetary disks [*Visser et al.*, 2007], throughout our galaxy [*Flagey et al.*, 2006], in neighboring galaxies [*Sajina et al.*, 2007], and in Titan's atmosphere [*Coates et al.*, 2007]. Solar system PAH abundances can be derived from examination of meteorites, particularly carbonaceous chondrites, with the most common PAH species being 2-, 3-, and 4-ring structures such as naphthalene, phenanthrene, anthracene, pyrene, and chrysene [*Zolotov and Shock*, 2001]. PAH concentrations of 15–38 ppm are found in the Murchison meteorite where the most abundant forms are phenanthrene, carbazole, fluoranthene, pyrene, chrysene, perylene, benzo-perylene and coronene [*Sephton et al.*, 2004].

[3] Comets, meteorites, micrometeorites, and ISM dust deliver significant quantities of organic material including PAHs to the surfaces of Mercury, Venus, Earth, and Mars [*Chyba and Sagan*, 1992; *Flynn*, 1996]. However, the Viking landers failed to detect organic compounds in the upper few centimeters of the regolith at ppb levels [*Biemann et al.*, 1977]. This unexpected result led to theories postulating destruction of in-fall material by direct or indirect damage from ionizing radiation [*Hunten*, 1979; *Benner et al.*, 2000]. Theoretical calculations of the distribution of reactive oxygen species [*Zent and McKay*, 1994] and attenuation of radiation damage as a function of depth [*Kminek and Bada*, 2006; *Dartnell et al.*, 2007] predict survival of organics starting approximately one meter below the surface of the regolith.

[4] In 2003 the European Space Agency (ESA) launched Mars Express with a primary goal of acquiring orbital remote sensing data detailing Mars geomorphology and geochemistry [*Vago et al.*, 2006]. The mission also deployed a lander, Beagle 2, with an instrument package designed to search for bio-organic compounds [*Chicarro et al.*, 2003; *Wright et al.*, 2003]. While the orbital mission continues to provide significant information, contact was lost with Beagle 2 during descent. As a precursor to future scientific missions to Mars such as sample return and human exploration, ESA is developing the ExoMars rover mission for an in situ search for evidence of past or present near subsurface biological activity. ExoMars instrumentation includes the mast-mounted PanCam, infrared and Mossbauer spectrometers, ground-penetrating radar, and a microscope. The rover will deploy a drill capable of retrieving samples from a depth of 2 meters. Instruments searching for organics include a Raman laser induced breakdown spectrometer (Raman-LIBS), microchip capillary electrophoresis, a laser desorption ion source with GC-mass spectrometer, an X-ray diffractometer, and a life marker chip capable of identifying PAH targets such as naphthalene, pyrene, and coronene [*Parnell et al.*, 2007]. The fiberoptic head for the Raman-LIBS and a medium resolution camera on the robotic arm permit close examination of surface formations. Unfortunately, the presently planned organic detection instrumentation requires either sample destruction and/or consumption of limited chemical resources.

[5] In exploration of extreme environments on Earth it has proven useful to employ a preliminary triage effort using probes requiring only renewable energy before invoking resource-intensive techniques [*Storrie-Lombardi*, 2005]. Native fluorescence is the single most sensitive active photonic imaging probe for detecting aromatic organic compounds that does not require sample prepara-

[1]Kinohi Institute, Altadena, California, USA.
[2]Mullard Space Sciences Laboratory, Department of Space and Climate Physics, University College London, Holmbury St. Mary, UK.
[3]Also at Centre for Planetary Sciences, University College London, London, UK.
[4]College of Ocean and Atmospheric Sciences, Oregon State University, Corvallis, Oregon, USA.

Table 1. Peridotite Composition Compared to the Mars Chassigny Meteorite

| Rock Type | Origin and Description | Partial Chemical Composition (Oxide wt. %) | | | | Olivine (Vol. %) |
		SiO_2	FeO	MgO	Cr_2O_3	
Peridotite	Nickel Mountain[a]	43	10	45	0.79	90
Chassigny	Mars, SNC,[b] olivine-rich	37	27	33	0.83	88

[a]Riddle, Oregon, USA [*Pecora and Hobbs*, 1942].
[b]Shergotty-Nakhla-Chassigny meteorites [*Prinz et al.*, 1974].

tion, expenditure of limited reagents, or target destruction and has been proposed as a potential survey tool for Mars exploration [*Storrie-Lombardi et al.*, 2001; *Nealson et al.*, 2002]. Near UV (350–380 nm) excitation of small aromatic organic molecules including 3-, 4-, and 5-ring PAHs produces fluorescence in the visible spectrum making PanCam fluorescence imaging feasible. Epifluorescent photomicrograph detection limits of 10 ng/cm^2 have been reported for 3- and 4-ring PAHs in the laboratory [*Fisher et al.*, 1998] and 0.02 to 0.2 $\mu g/L$ in the field for 3-, 4-, and 5-ring structures [*Karlitschek et al.*, 1998].

[6] We investigate here the possibility that extending PanCam information gathering into the UV with addition of a 365 nm light source might provide ExoMars with a triage capability to search for regolith organics. We propose that constraints on preservation of organic material as a function of depth can be derived from PanCam epifluorescence images of drill cuttings.

2. Methods and Materials

[7] The Beagle 2 stereo camera system provides wide-angle (34° field of view, 0.58 mrad/pixel), stereo, multi-spectral imaging of the area around the lander [*Griffiths et al.*, 2005]. Its 1024 × 1024 pixel CCD is sensitive to wavelengths between 400 and 1000 nm. Three filters selected for this study exhibit center wavelengths of 448, 530, and 655 nm with full-width-at-half-maximum (FWHM) pass bands of 25, 40, and 31 nm, respectively. For our experiments a Foculus FO432SB camera (1.4 Mpixels, 16-bits/pixel greyscale, 56dB SNR, Fujinon HF25HA-1 25 mm focal length 63° FoV lens, exposure time 1 μs to 65 s) was interfaced to the flight-spare Beagle 2 filter-wheel.

[8] A peridotite from Nickel Mountain, Riddle, Oregon, U.S.A. [*Pecora and Hobbs*, 1942] was selected as an analog for the olivine- and phyllosilicate-rich Martian regolith thought present in the Nili Fossae region [*Poulet et al.*, 2005]. The sample, exhibiting olivine abundance similar to the Chassigny SNC meteorite (Table 1) and containing ~5% phyllosilicate (serpentine), was pulverized between steel and alumina plates, and sieved to produce the less than 300 μm particle fraction used in this study.

[9] PAH targets were produced using 99% pure solutions of anthracene (in acetone 1 $\mu g/\mu L$), pyrene (in methanol 1 $\mu g/\mu L$), and perylene (in methylene chloride 2 $\mu g/\mu L$) obtained from Sigma-Aldrich Pharmaceuticals, Inc. For detection limit experiments aliquots of peridotite soil were doped with each PAH species at 50 ± 5 ppm. To mimic the optical detection challenge presented to PanCam on the Mars surface (monitoring loose fine material such as drill cuttings) doped peridotite grain samples were illuminated after being placed without packing against an optically thick bed of un-doped peridotite grains.

[10] UV excitation source was a 365 nm Nichia LED (NSHU590B) with average optical output power of 1.4 mW, spectrum FWHM of 10 nm, effective operating temperature −30 to 85°C, and 10° beam divergence. Decrease in photon flux as a result of divergence constrains the LED-to-target distance. Source-to-target distance was 1 meter for experiments reported here.

3. Experiments and Results

[11] Experiment 1: Ten UV-Vis-NIR fluorescence emission spectra for peridotite targets doped with 3-ring anthracene, 4-ring pyrene, or 5-ring perylene were obtained with an Ocean Optics 2000 fiberoptic spectrometer. Mean spectra (n = 10, un-doped peridotite spectrum subtracted) appear in Figure 1. Table 2 summarizes spectral character-istics. Fluorescence emission shifts to longer wavelengths with increasing number of rings. Spectral power distribu-
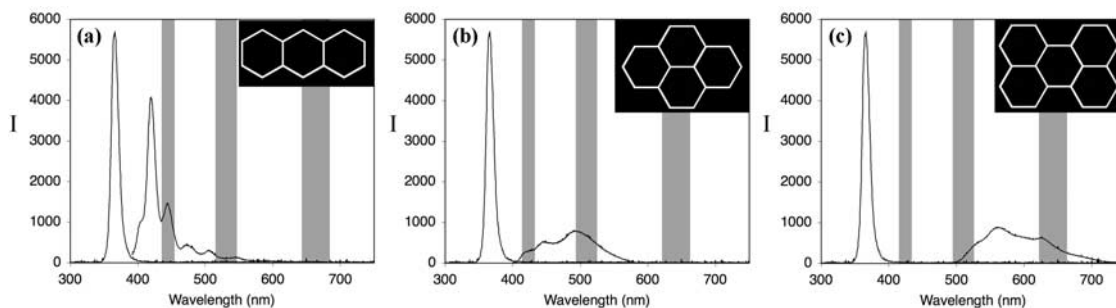

Figure 1. Fluorescence response to 365 nm excitation for (a) anthracene, (b) pyrene, and (c) perylene. Blue, green, and red filter FWHM bands appear in gray. The spectra predict anthracene will be detected primarily in blue and, to a lesser extent, green filter bands, pyrene in blue and even more efficiently in green, and perylene in green and red bands. Only the green band is sensitive to fluorescence from all three targets.

Table 2. Fluorescence Response Characteristics of Three PAHs Following 365 nm LED Excitation

	Molecular Characteristics			Spectra[a]			Image (ΣGs)[b]		
PAH	Rings	Formula	GMW[c]	B_{50}[d] (nm)	Max (nm)	R_{50}[d] (nm)	Blue	Green	Red
Anthracene	3	$C_{14}H_{10}$	178.2	401	421	457	3.1	1.3	0
Pyrene	4	$C_{16}H_{10}$	202.3	425	500	535	2.5	3.1	0
Perylene	5	$C_{20}H_{12}$	252.3	519	565	669	0.1	2.4	1.0

[a]Spectra are depicted in Figure 1.

[b]Values are relative to ΣGs for red band perylene. Surface plots are depicted in Figure 2.

[c]Gram molecular weight.

[d]B_{50} and R_{50} are the wavelengths bounding 50% of the integrated power of the fluorescence spectral response.

tions predict anthracene will be most efficiently detected in blue and green filter bands; pyrene most easily detected in green and to a slightly lesser degree in blue; and perylene should be most easily detected in green with some activity in red. The green band signal should be unaffected by the ~1% of the 365 nm LED excitation energy contaminating the blue band. Spectral data predict only the green band will efficiently detect all three PAH species.

[12] Experiment 2: Fluorescent images of the three PAH-doped peridotite granular targets were obtained using blue, green, and red filters (65s exposure; distance 1 meter). Surface plots of gray scale values for doped peridotite grain fluorescence (Figure 2) agree with spectral data. Anthracene fluorescence is easily detected in (a) blue and (b) green filter bands, but not in (c) red. Pyrene is also detected in (d) blue and (e) green bands, but not in (f) red. Perylene is not seen in (g) blue, but is detected in (i) green and (j) red. Table 2 summarizes relative total fluorescent emission normalized to perylene detection in red. Imaging confirms the spectral prediction that only the green band efficiently detects all three PAH molecular species.

[13] Experiment 3: Clusters of pyrene-doped peridotite grains were deposited at six sites on the surface of a background bed of un-doped peridotite with total pyrene doses of 4, 8, 12, 16, 20 and 24 μg. Images were obtained with 65s exposure at a distance of 1 meter. All determinations were performed in triplicate. Fluorescence response to excitation is defined as the sum of target grayscale values ($\mathbf{I} = \Sigma Gs$) where a pixel gray scale value (Gs) is greater than 6σ above background. Figure 3 depicts $\mathbf{I}$ for green band detection as a function of total pyrene target dose. Detection limit, defined as x-axis intercept (where $\Sigma G_s = 0$), is 1.5 μg. Error bars are 6σ variance for triplicate determinations.

4. Discussion and Conclusions

[14] Multiple factors affect PAH fluorescence detection limits. First, PAH molecules are inherently "sticky". Adherence to regolith dust grains rich in iron oxides would impair photonic detection since these oxides absorb both UV excitation and longer wavelength emission photons. However, this adhesive characteristic increases the likelihood that nanometer to micrometer scale PAH in-fall will cluster into significantly larger clumps producing photonic "hot spots" either at random regolith sites or in cracks and crevices of surface rocks or outcrops [*Storrie-*
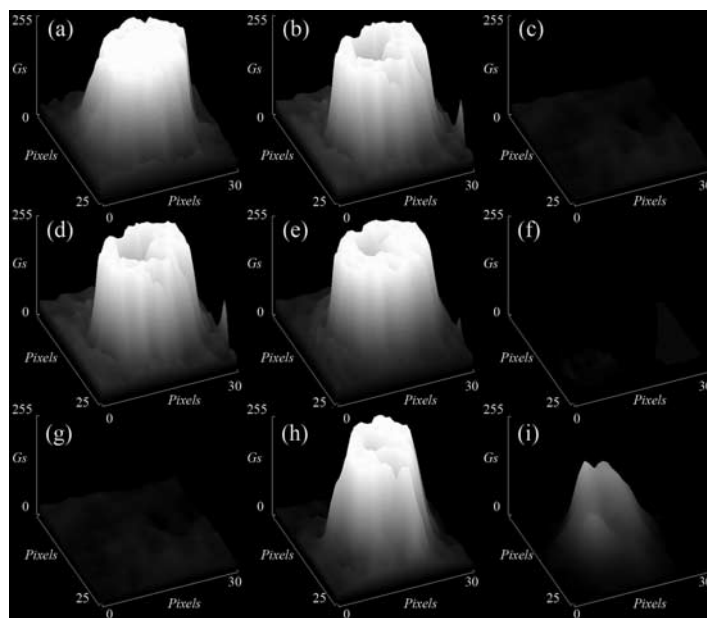

Figure 2. Surface plots of pixel gray scale values for peridotite grains doped with 20 μg of three PAH species. Excitation at 365 nm produces fluorescence in anthracene detected using (a) blue and (b) green PanCam filters, but not with (c) red. Pyrene is also detected in both (d) blue and (e) green bands, but not in (f) red. Perylene is not detected in (g) blue, but is readily detected in (h) green and (i) red bands.
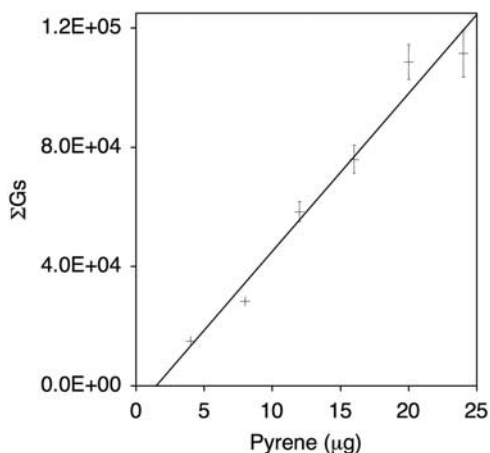
Figure 3. Fluorescence detection limits following 365 nm excitation of pyrene-doped peridotite for PanCam green band at a camera to target distance of 1 meter. Detection limit, defined as x-axis intercept where total integrated gray scale value ($\mathbf{I}$) = 0, occurs at 1.5 μg total pyrene. Error bars are 6σ variation for triplicate determinations at each doping site.

Lombardi et al., 2001]. Such variance in spatial distribution may occur within a single drill site. Organic clustering is a clear advantage for photonic detection. During chemical assays, grinding and dissolving samples blends target concentration variance to a single mean value destroying target spatial distribution information and eliminating localized signal maxima.

[15] The second major constraint on detection is excitation photon flux at target. Whether to deploy a UV LED or laser diode will ultimately be determined by engineering constraints. We demonstrate here that significant science can be accomplished using a simple 365 nm LED at a distance of 1 meter. Attachment of one LED to the rover arm would be sufficient for rapid imaging. Even though we were able to acquire adequate signals using a single LED at 1 meter distance from PAH targets in this study, mounting a single LED on the rover mast 1.5 meters above the regolith surface and 2 meters from the drill cuttings will significantly reduce target illumination. Mounting a UV laser diode on the mast would significantly decrease exposure times, eliminate blue band contamination, enhance instrument sensitivity, increase remote sensing and provide the best means of ensuring that any target visible to PanCam can be illuminated.

[16] Finally, camera spatial resolution significantly impacts fluorescence detection limits. The ExoMars PanCam system includes not only the mast-mounted wide angle cameras (WAC) discussed in this work, but also a high-resolution (85 μrad/pixel) mast-mounted camera (HRC) producing 'zoom' images with 5° field of view [*Griffiths et al.*, 2006] and a rover arm-mounted Close-Up Imager (CLUPI), providing 3.4 μm resolution at 10 cm working distance. Fluorescent images obtained with HRC and CLUPI could significantly increase PAH detection limits beyond the results reported here. It should be noted that organic fluorescence is distinguished from mineral fluorescence by the gradual decay of the fluorescence signature once organic ring structures are exposed to Mars surface radiation. In like fashion, living biota can be distinguished from PAHs by the ability to repair ionizing damage if protected and provided with sources of water and energy. Use of the probe would be most efficient if it is employed during the hour after sunset when drilling has stopped for the day, power is relatively abundant, drill cuttings are still fresh, and ambient light is minimized.

[17] Addition of UV illumination is a logical extension of remote site survey and drill monitoring tasks of WAC, HRC, and CLUPI. While the primary scientific task for fluorescence imaging are drill sample triage to identify sites rich in organic in-fall, the technology readily lends itself to other lower probability but high-payoff experiments. 365 nm excitation produces fluorescence in biomolecules common to Earth microbial life including species inhabiting Mars analog extreme environments [*Warren-Rhodes et al.*, 2006]. Primary targets include metabolic enzymes such as nicotinamide adenine dinucleotide (NADH) and flavin adenine dinucleotide (FAD); photosynthetic pigments; and diagenetic products of microbial life. FAD and NADH fluorescence changes with oxidation state making possible in situ remote sensing of metabolic activity [*Storrie-Lombardi*, 2005].

[18] Epifluorescent imaging of organics is not limited to UV excitation. 660 nm excitation of cyanobacteria photosynthetic pigments produces fluorescence at 700–750 nm, a response readily detected by PanCam. While discovery of recent or extant life within the first two meters of Mars regolith or hidden in UV-protected crevices of an outcrop is highly improbable, such a finding would significantly alter our view of life in the cosmos. In summary, the deployment of a low mass UV photonic probe for remote detection of fundamental organic and biogenic material is a low-risk, high-gain triage option for the ExoMars mission.

References

Benner, S. A., K. G. Devine, L. N. Matveeva, and D. H. Powell (2000), The missing organic molecules on Mars, *Proc. Natl. Acad. Sci. U. S. A.*, *97*, 2425–2430.

Biemann, K., et al. (1977), The search for organic substances and inorganic volatile compounds in the surface of Mars, *J. Geophys. Res.*, *82*, 4641–4658.

Chicarro, A., P. Martin, and R. Trautner (2003), Mars Express: Unraveling the scientific mysteries of the red planet, *ESA Bull.*, *115*, 18–25.

Chyba, C., and C. Sagan (1992), Endogenous production, exogenous delivery and impact shock synthesis of organic molecules: An inventory for the origins of life, *Nature*, *355*, 125–132.

Coates, A. J., F. J. Crary, G. R. Lewis, D. T. Young, J. H. Waite Jr., and E. C. Sittler Jr. (2007), Discovery of heavy negative ions in Titan's ionosphere, *Geophys. Res. Lett.*, *34*, L22103, doi:10.1029/2007GL030978.

Dartnell, L. R., L. Desorgher, J. M. Ward, and A. J. Coates (2007), Modelling the surface and subsurface Martian radiation environment: Implica-

tions for astrobiology, *Geophys. Res. Lett.*, *34*, L02207, doi:10.1029/2006GL027494.

Ehrenfreund, P., and S. B. Charnley (2000), Organic molecules in the interstellar medium, comets, and meteorites: A voyage from dark clouds to the early Earth, *Annu. Rev. Astron. Astrophys.*, *38*, 427–483.

Fisher, M., V. Bulatov, S. Hasson, and I. Schechter (1998), Fast aerosol analysis by Fourier transform imaging fluorescence microscopy, *Anal. Chem.*, *70*, 2409–2414.

Flagey, N., F. Boulanger, L. Verstraete, M. A. Miville Deschênes, A. Noriega Crespo, and W. T. Reach (2006), Spitzer/IRAC and ISOCAM/CVF insights on the origin of the near to mid-IR Galactic diffuse emission, *Astron. Astrophys.*, *453*, 969–978.

Flynn, G. J. (1996), The delivery of organic matter from asteroids and comets to the early surface of Mars, *Earth Moon Planets*, *72*, 469–474.

Griffiths, A. D., A. J. Coates, J.-L. Josset, G. Paar, B. Hofmann, D. Pullan, P. Rüffer, M. R. Sims, and C. T. Pillinger (2005), The Beagle 2 stereo camera system, *Planet. Space Sci.*, *53*, 1466–1482.

Griffiths, A. D., A. J. Coates, R. Jaumann, H. Michaelis, G. Paar, D. Barnes, and J.-L. Josset (2006), Context for the ESA ExoMars rover: The Panoramic Camera (PanCam) instrument, *Int. J. Astrobiol.*, *5*, 269–275.

Hunten, D. M. (1979), Possible oxidant sources in the atmosphere and surface of Mars, *J. Mol. Evol.*, *14*, 71–78.

Karlitschek, P., F. Lewitzka, U. Bunting, M. Niederkruger, and G. Marowsky (1998), Detection of aromatic pollutants in the environment by using UV-laser-induced fluorescence, *Appl. Phys. B*, *67*, 487–504.

Kminek, G., and J. L. Bada (2006), The effect of ionizing radiation on the preservation of amino acids on Mars, *Earth Planet. Sci. Lett.*, *245*, 1–5.

Nealson, K. H., A. Tsapin, and M. Storrie-Lombardi (2002), Searching for life in the universe: Unconventional methods for an unconventional problem, *Int. Microbiol.*, *5*, 223–230.

Parnell, J., et al. (2007), Searching for life on Mars: Selection of molecular targets for ESA's aurora ExoMars mission, *Astrobiology*, *7*, 578–604.

Pecora, W. T., and S. W. Hobbs (1942), Nickel deposit near Riddle, Douglas County, Oregon, *U.S. Geol. Surv. Bull.*, *931*, 205–206.

Poulet, F., J.-P. Bibring, J. F. Mustard, A. Gendrin, N. Mangold, Y. Langevin, R. E. Arvidson, B. Gondet, and C. Gomez (2005), Phyllosilicates on Mars and implications for early Martian climate, *Nature*, *438*, 623–627.

Prinz, M., P. H. Hlava, and K. Keil (1974), The Chassigny meteorite: A relatively iron-rich cumulate dunite, *Meteoritics*, *9*, 393–394.

Sajina, A., L. Yan, L. Armus, P. Choi, D. Fadda, G. Helou, and H. Spoon (2007), Spitzer mid-infrared spectroscopy of infrared luminous galaxies at z ~ 2. II. Diagnostics, *Astrophys. J.*, *664*, 713–737.

Sephton, M. A., G. D. Love, J. S. Watson, A. B. Verchovsky, I. P. Wright, C. E. Snape, and I. Gilmour (2004), Hydropyrolysis of insoluble carbonaceous matter in the Murchison meteorite: New insights into its macromolecular structure, *Geochim. Cosmochim. Acta*, *68*, 1385–1393.

Storrie-Lombardi, M. C. (2005), Post-Bayesian strategies to optimize astrobiology instrument suites: Lessons from Antarctica and the Pilbara, in *Astrobiology and Planetary Missions*, edited by R. B. Hoover, G. V. Levin, and A. Y. Rozanov, *Proc. SPIE Int. Soc. Opt. Eng.*, *5906*, 288–301.

Storrie-Lombardi, M. C., W. F. Hug, G. D. McDonald, A. I. Tsapin, and K. H. Nealson (2001), Hollow cathode ion lasers for deep ultraviolet Raman spectroscopy and fluorescence imaging, *Rev. Sci. Instrum.*, *72*, 4452–4459.

Vago, J., B. Gardini, G. Kminek, P. Baglioni, G. Gianfiglio, A. Santovincenzo, S. Bayon, and M. van Winnendael (2006), Searching for life on the red planet, *ESA Bull.*, *126*, 16–23.

van Dishoeck, E. F. (2004), ISO spectroscopy of gas and dust: From molecular clouds to protoplanetary disks, *Annu. Rev. Astron. Astrophys.*, *42*, 119–167.

Visser, R., V. C. Geers, C. P. Dullemond, J. C. Augereau, K. M. Pontoppidan, and E. F. van Dishoeck (2007), PAH chemistry and IR emission from circumstellar disks, *Astron. Astrophys.*, *466*, 229–241.

Warren-Rhodes, K. A., K. Rhodes, S. Pointing, S. Ewing, D. Lacap, B. Gomez-Silva, R. Amundson, E. I. Friedmann, and C. P. McKay (2006), Hypolithic cyanobacteria, dry limit of photosynthesis and microbial ecology in the hyperarid Atacama Desert, *Microbial Ecol.*, *52*, 389–398.

Wright, I. P., M. R. Sims, and C. T. Pillinger (2003), Scientific objectives of the Beagle 2 lander, *Acta. Astronaut.*, *52*, 219–225.

Zent, A. P., and C. P. McKay (1994), The chemical-reactivity of the Martian soil and implications for future missions, *Icarus*, *108*, 146–157.

Zolotov, M. Y., and E. L. Shock (2001), Stability of condensed hydrocarbons in the solar nebula, *Icarus*, *150*, 323–337.

_____

A. J. Coates, A. D. Griffiths, and J.-P. Muller, Mullard Space Sciences Laboratory, Department of Space and Climate Physics, University College London, Holmbury St. Mary RH5 6NT, UK.

M. R. Fisk, College of Ocean and Atmospheric Sciences, Oregon State University, Corvallis, OR 97331, USA.

M. C. Storrie-Lombardi, Kinohi Institute, 1700 Alta Wood Drive, Altadena, CA 91001, USA. (mike@kinohi.org)